Journal of
Engineering Sciences
Faculty of Engineering
Assiut University
JES
مجلة
العلوم الهندسية
كلية الهندسة
جامعة أسيوط
journal homepage: http://jesaun.journals.ekb.eg

Numerical Study of the Effect of using a Small Fence through the Flow Passage on the Performance of a Langston Turbine Cascade

Received 31 January 2025; Revised 19 June 2025; Accepted 19 June 2025

Mostafa K. Soliman [1]
Magdy A. Bassily [2]
Ramadan Bassiouny [3]
Gamal R. H. Abo Elyamin[4]

Keywords
Turbine cascade, Total pressure loss, CFD, Fence

Abstract: The present study computationally investigates the steady incompressible flow behavior through Langston turbine cascade. A three-dimensional numerical model was developed by ANSYS-Fluent software. The model solves the RANS governing equations along with the transition-SST (4eq.) model. The results of the model have been validated using experimental data obtained by Langston. A proposed configuration to improve the turbine performance is adopted using fence mounted close to the leading edge. The function of the fence is to reduce the pressure losses and accordingly improve the turbine performance. The results showed that the total pressure loss coefficient decreased by 5.244 % according to fence addition. The fence effectively disrupted the horseshoe vortex and modified the pressure flow field, leading to a weakened passage vortex and suppressed secondary flow. Adding a fence resulted in an enhancement of the flow uniformity and reduction of the vortex strength with improvements in the aerodynamic efficiency of the turbine cascade.

1. Introduction

The turbine efficiency is an important measure for turbine performance. In turbines, secondary flow losses are generated through the flow passage between turbine blades that negatively affect the efficiency. The blade's thickness, passage curvature, and rotational speed are parameters that affect these losses generation. In gas turbines almost 33 percent of the total losses are related to the secondary flow losses [1]. Secondary flow losses and profile losses mechanisms cause the generation of more than 60% of the total losses in turbines [2, 3]. The pressure gradient and its effect on the incoming end wall boundary layers cause the most increment in secondary flow in turbomachinery blade rows. Langston et al. [4] reported that high pressure gradients are generated inside the passage. It is

[1] Senior Engineer at Egyptian Railways, El-Minia Sector, Egypt. mokasoliman1985@gmail.com
[2] Emeritus prof., Mechanical power Engineering and Energy Dept., Faculty of Engineering, Minia University, Egypt. magdy_bassily@yahoo.com
[3] Professor, Mechanical power Engineering and Energy Department, Faculty of Engineering, Minia University., Egypt. ramadan.b@mu.edu.eg
[4] Lecturer, Mechanical power Engineering and Energy Department, Faculty of Engineering, Minia University, Egypt. gamalrabeh@mu.edu.eg

https://doi.org/ 10.21608/jesaun.2025.356918.1417

concluded that the end wall boundary layer begins inside the cascade passage behind the end wall separation line that related to the suction side. The fluid in this boundary layer which locates near the pressure side flows across the end wall towards the suction surface. At the cascade end wall, the inlet boundary layer separation starts at the saddle-point and forms the horseshoe vortex, figure 1 [3]. The horseshoe vortex consists of two different vortices one of them is the passage vortex formed by the cross-pressure gradient into the passage towards the suction side; the other leg is extracted into the adjacent passage and becomes a counter vortex. Another significant rise in the losses is resulted from the flow separation which formed at the trailing edge and behind the cascade.

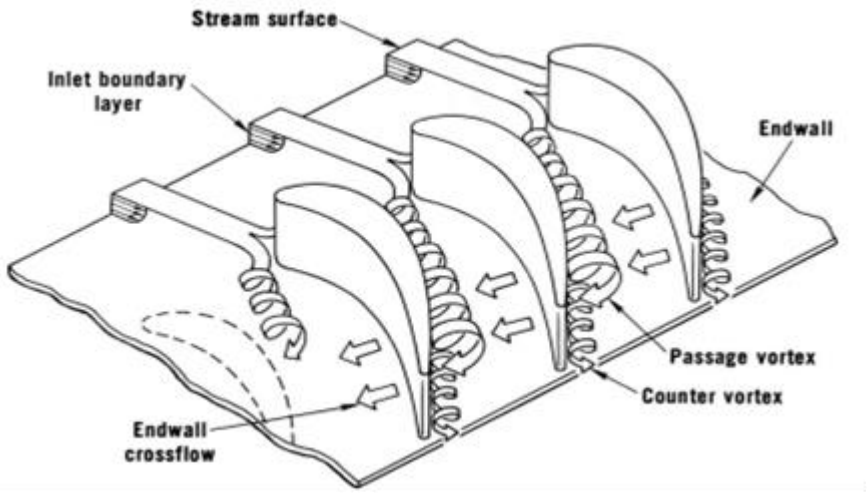

Fig. 1 Three-dimensional separation of boundary layer entering a planar turbine cascade [3]

Many previous researches focused on techniques to reduce the turbine secondary flow losses to enhance the turbine efficiency. One of these techniques is adopting end wall fences. The impact of using end wall fences is to stop the cross-passage flow from the pressure side to the suction side. 3-D flow in turbine cascades without and with fence is investigated by different researchers. The formation of streamwise vortex in turbine cascade was studied using end wall fence [6]. Govardhan et al. [7] mounted one streamwise fence to suppress and change the migration of the pressure side leg of the horseshoe vortex. Kumar and Govardhan [8] analysed the flow topology in a turbine cascade with and without fence, highlighting vortex structures and their influence on aerodynamic performance. Adeola et al [9] investigated experimentally the results of axial vortices, flow deviation angles, and total pressure loss coefficients near the end wall in a passage of the linear cascade. Cui et al. [10] investigated the reduction in aerodynamics loss characteristics in low pressure turbine cascade after the leading-edge optimization. Aunapu [11] optimized boundary layer fence by using two techniques to modify the end wall secondary flow, specifically the path of the passage vortex. During the past few years, significant improvements have been achieved in the design of different small-scale surface features such as riblets, dimples, grooves, etc. used in gas turbine [12]. The impact of end wall profiling on secondary flow and loss development in a turbine cascade is discussed by Ingram et al. [13, 14]. The impact of turbine blade tip shape on total pressure losses and secondary flow losses of a linear turbine cascade was investigated [15]. The trailing edge sweep was applied to the turbine stage to investigate its effect on the flow at cascade exit in [16]. It is concluded that the turbine stage

achieves an efficiency enhancement by 0.4%. Halder et al. [17] carried out an optimization of blade leading edge and trailing edge ratio in impulse turbine using ANSYS-CAD design. The results indicated that the suggested design enhanced the peak efficiency and torque by 3.4 % and 2 %; respectively.

The aim of the current study is to investigate computationally the impact of having a fence, located near the saddle point in a linear turbine cascade, on the total pressure loss coefficient, which presents the loss generation level. The commercial software ANSYS-FLUENT 2023 R1 is utilized to simulate the problem. Experimental validation has been carried out depending on the experimental results from Langston et al. [4].

2. Problem description and Solution Methodology

The problem to be studied is the flow pattern through Langston turbine cascade to depict the regions where high-pressure losses exist. Hence, a remedy is sought for this problem as a way to improve the turbine efficiency. As a numerical visualization of the flow structure through Langston turbine cascade, the computational fluid dynamics tool is used to predict this flow pattern. ANSYS-FLUENT 2023 R1 has been used to solve for the governing equations of flow through this type of turbine blades. It enables detailed visualization and quantification of flow parameters, allowing for comprehensive evaluations of different design modifications. Figure 2 (a) displays the physical domain of interest of Langston turbine cascade and different sections, as plotted by Langston et al. [4]. Due to periodicity, a single blade is selected and built to generate a 3D mesh configuration as shown in Fig. 2(b). The geometric dimensions of the studied turbine blade are listed in Table (1). In this numerical study, air was the working fluid with viscosity of 1.7894×10^{-5} kg/m. s, and density of 1.122 kg/m^3 at STP conditions. All computational runs were carried out with inlet air angle of 44.7^o parallel to the mainstream of the cascade set. The upstream inlet velocity, U_o, was 33.5 m/s corresponding to inlet and exit Reynolds numbers based on blade axial chord of 5.9×10^5 and 10^7; respectively. In the preprocessing stage, boundary conditions have been set as inlet velocity, inlet temperature, no slip conditions at walls, and periodic boundary conditions at mid-span between blades.

Table 1: Cascade geometry data

Axial chord, mm	span/axial chord	Chord/axial chord	Pitch/axial chord	Inlet camber line angle	outlet camber line angle
281.3	0.9888	1.2242	0.9555	43.99^o	25.98^o

A structured O-grid topology was generated around the blade using ICEM meshing software. The mesh consisted of hexahedral cells as show in figure 2(b). The near-wall grid spacing is 10^{-6} b_x that provides the value of y+ about and below unity throughout the walls. The ANSYS-Fluent 2023R1 CFD software was used to solve the steady-state incompressible Reynolds-Averaged Navier-Stokes (RANS) equations using the finite volume method. The governing partial differential equations, listed below, are discretized using the finite volume approach to develop the algebraic equations of the computation domain to be solved in the processing steps.

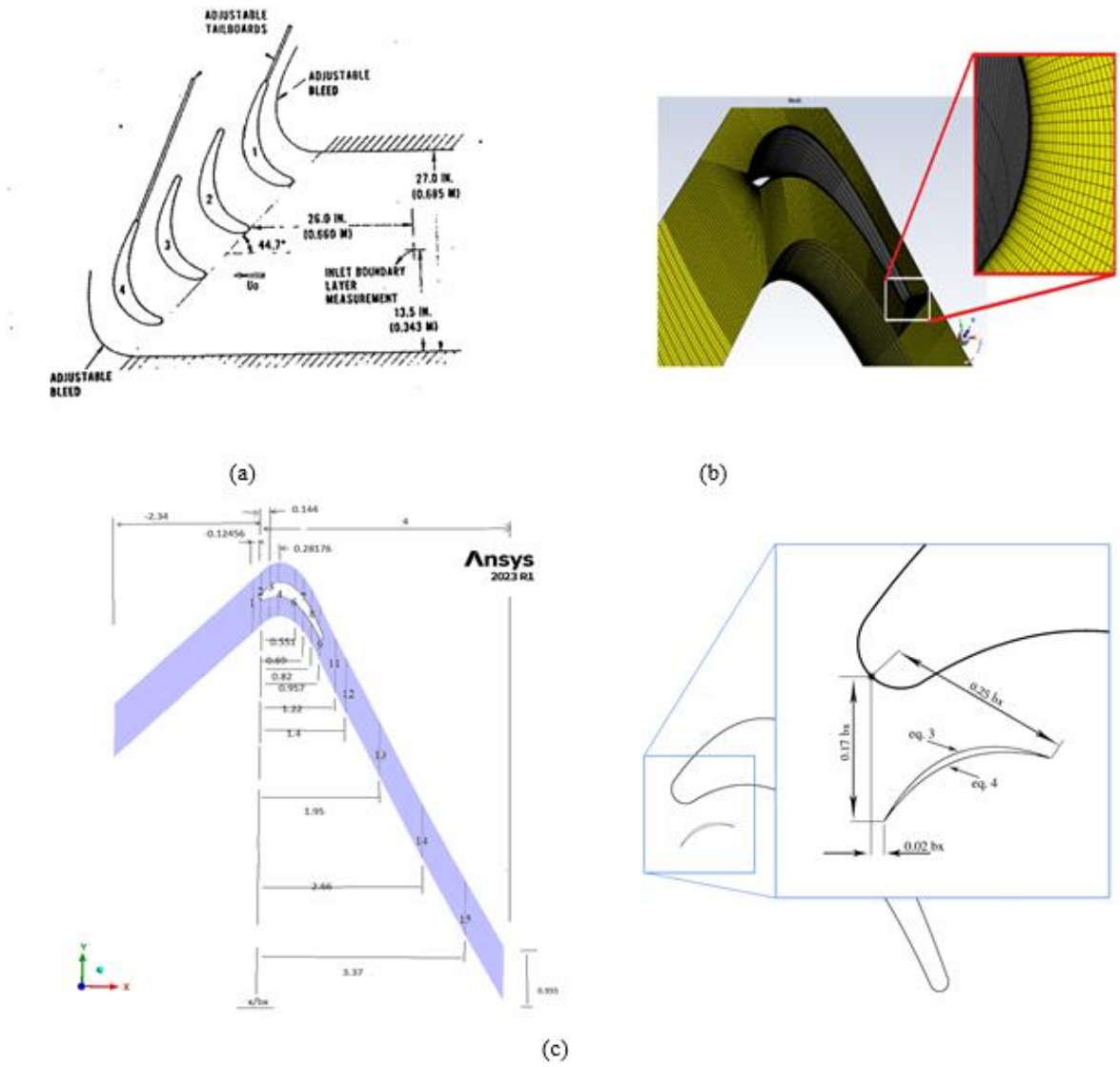

Fig. 2 Cross section view of cascade geometry and different sections [4]
a) Physical domain b) Computational grid (c) Domain with fence

Conservation of mass equation:

$$\frac{\partial}{\partial x_i}(\rho u_i) = 0 \qquad (1)$$

Conservation of momentum equation:

$$\rho\left(\frac{\partial u_i}{\partial t} + u_j\frac{\partial u_i}{\partial x_j}\right) = -\frac{\partial P}{\partial x_i} + \frac{\partial}{\partial x_j}\left(\mu\left(\frac{\partial u_i}{\partial x_j} + \frac{\partial u_j}{\partial x_i}\right) - \rho\overline{u}_i\overline{u}_j\right) \qquad (2)$$

The transition-SST turbulence model is adopted to predict the turbulence kinetic energy and secondary flow through the passage based on the model equations from reference [18]. Ahmed Abdelnaby et al. presented a study of the heat transfer area of heater tubes and its effect on the thermal efficiency of Stirling engines. Their results showed that elliptical tubes are superior to circular tubes. [19] While Ahmed Ibrahim et al. presented a numerical study of the film cooling effectiveness and flow field characteristics over a flat plate with an in-hole vortex generator.[20]. Ahmed Hussien et al. presented Comparative Investigation of the Energy Efficiency of Mini-Split Air Conditioning with Variable Refrigerant Flow Systems for Office Buildings in Hot Climate. [21]

Turbulent flow is clearly affected by the presence of walls, where the viscosity effect is largely considerable. The SST (4 eq.) model has provided good agreement with the measurement results. For the given boundary conditions, a uniform static pressure is applied at the domain exit section. The inlet turbulence intensity, I, is set to be 1 percent. The convective terms in the momentum equations are discretized by applying the second-order upwind scheme and the viscous terms of the second-order central differencing scheme. The coupled algorithm is employed for pressure-velocity coupling and all calculations are carried out in double-precision arithmetic. The numerical solution convergence stopping condition is set to be 10^{-5}. In the current study to reduce the losses generated in the cascade, many modification trials have been made in cascade passage geometry and blade profile. Some of these modifications lead to an insignificant improvement or even deterioration, hence, a proposed modification has been adopted in the present study using fence located near the saddle point. The impact of using fence is to block the cross-passage flow from pressure side to suction side. In the present study, the fence is used with height stretched from the lower end-wall to the upper one. The fences are located in such a way to affect the formation of horseshoe vortex (HSV), many trails have been made and best location is used in the present study. The arc of the fence is calculated based on equation (3) for the suction side and equation (4) for the pressure side.

$$y = -2E^{-06}x^4 + 0.0004x^3 - 0.044x^2 + 2.1226x - 61.118 \quad (3)$$

$$y = -1E^{-06}x^4 + 0.0003x^3 - 0.0329x^2 + 1.725x - 59.27 \quad (4)$$

3. Grid-Independency Test

In order to validate model results, a grid-independent test should be proved. This numerical experimentation has been carried out through trying four mesh configurations: grid (1) 1502514 cell, grid (2) 1874544 cell, grid (3) 2059754 cell, and grid (4) 2428868 cell. In figure 3 Mass-averaged loss coefficient ($\bar{C}_{pt}$) is presented for the four grids with different number of cells, to determine an optimal independent grid for flow simulation. The computation results are presented in figure 3 compared to the experimental measurements.
Grid convergence index (GCI) has been calculated for the 4 grids used in the current study and the values are shown in table 2. Figure 4 shows the convergence history of $\bar{C}_{pt}$ at exit based on the fine grid (grid 4).

Table 2: Grid convergence index (GCI)

Mesh level	No. of cells	Grid Refinement Ratios(r)= hfiner/hcoarser	Solution(Φ)= $\bar{C}$pt at plane 10	relative error(ϵ)=(Φfiner-Φcoarser)/ Φfiner	The order of convergence (p)	(GCI)= (Fs|ϵ|)/(rp−1)
Coarse	1874544	-	0.247793	-	p=[ln(ϵ32/ϵ21) /ln(r21)] = 5.71	-
Medium	2059754	r21 = 0.9152	0.245044	ϵ21 = −0.01122		0.0348
fine	2428868	r32 = 0.7999	0.243401	ϵ32 = −0.0975		0.0116

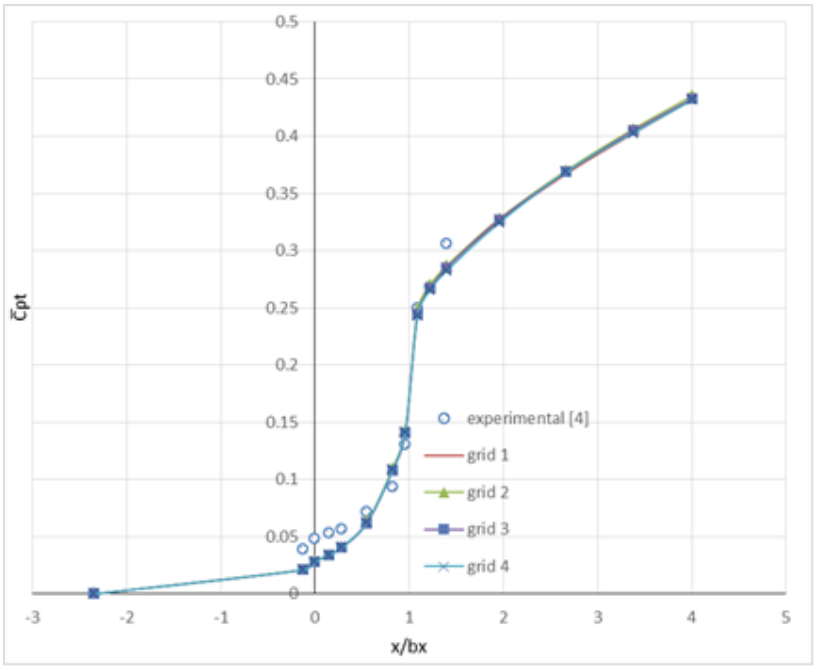

Fig. 3 Mass-averaged total loss coefficient $\bar{C}_{pt}$ as a function of axial distance through the cascade for different grids.

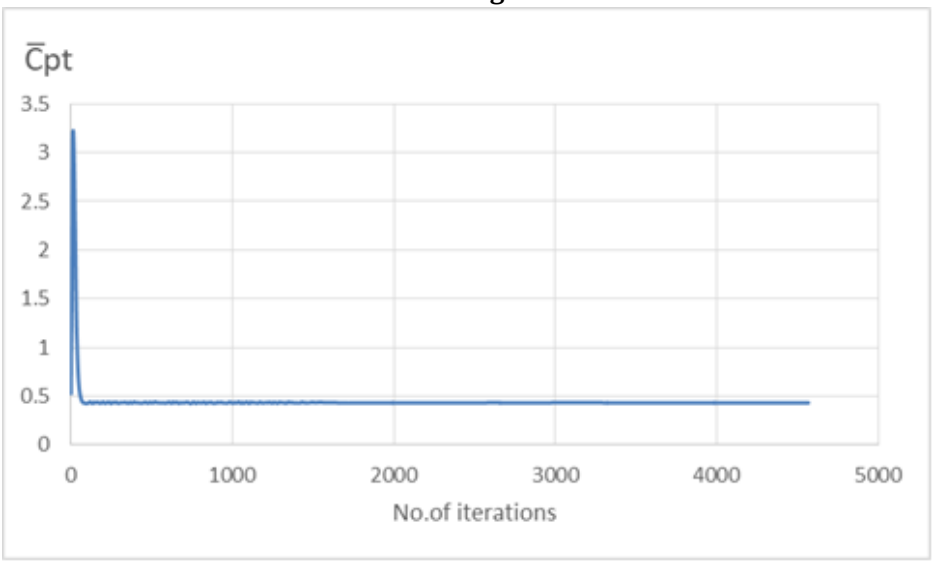

Fig. 4 Convergence history for $\bar{C}_{pt}$ at exit

4. Results and discussions

Validation for the model with published experimental measurements is discussed first. Then the flow patterns as well as the effect of using fence on secondary flow losses and pressure loss coefficient are discussed.

4.1. Validation

To make sure that the validation of the computational results, a comparison between the numerical simulations with the experimental one of [4] at different planes is presented in figure 5. The simulated contours of the total pressure loss coefficient and experimental data are on planes 3, 6, 9. Comparing the predicted contours to the measured ones shows a reasonable agreement at the selected planes.

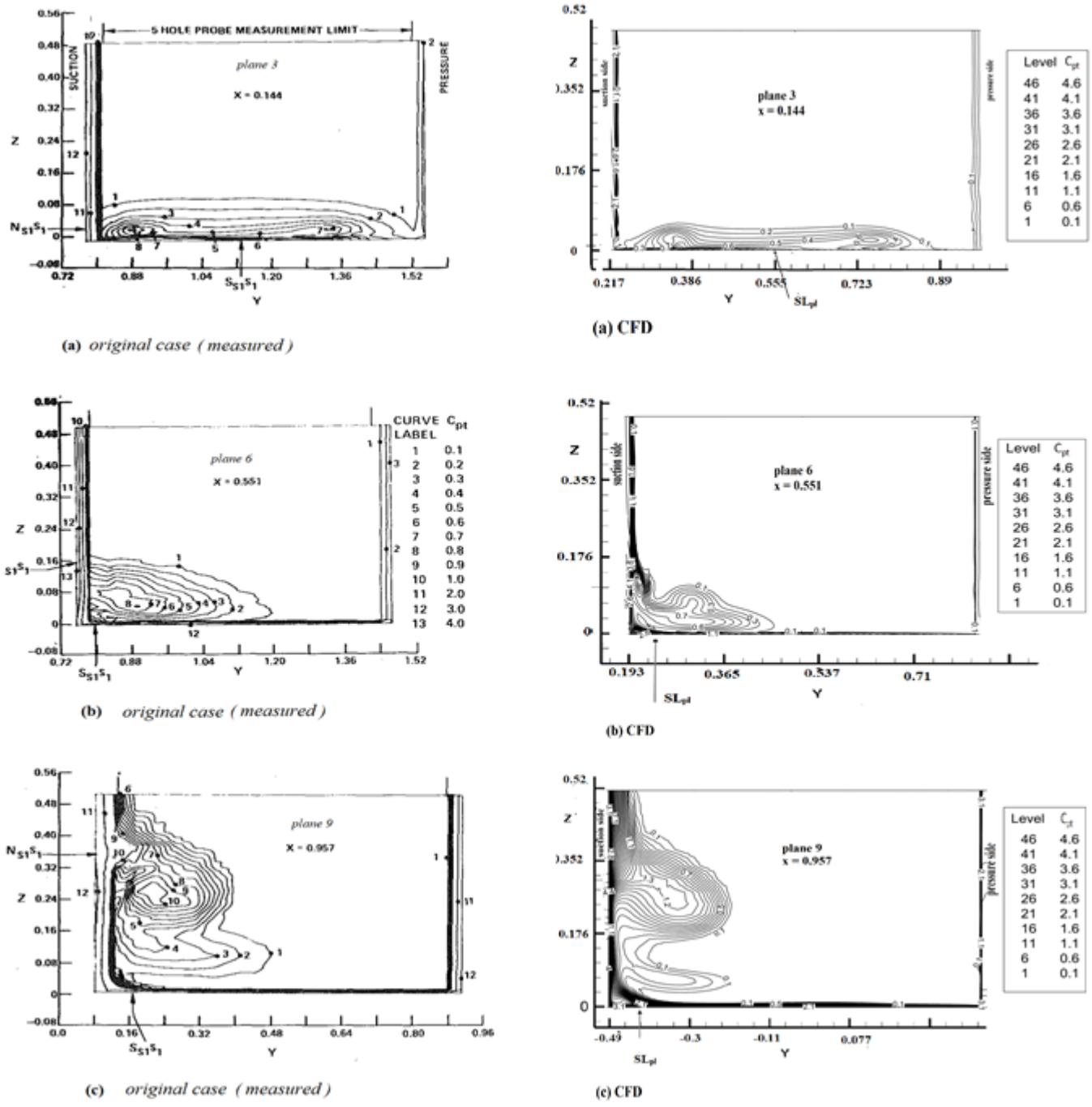

Fig. 5 Comparison between the calculated and the measured total pressure loss coefficient [4] at planes 3, 6, and 9

4.2. Flow stream-lines visualization

The visualized streamlines at the end wall of the passage as shown in figure 6 in case without using and with using a fence. The streamlines show the separation saddle point, (Sp). This saddle point of separation has two separation lines (SLpl) and (SLsl) which divide the entire flow field adjacent to the end wall into distinct regions of three-dimensional flow. The horseshoe vortex (HSV) is formed like that is formed in front of a cylinder that protrudes through the boundary layer on a flat plate. By analogy, it is shown in figure 6 one leg of the vortex (or three-dimensional separation) forms behind (SLpl) from the saddle point and along the adjacent blade suction surface. The indication of rotation is

that associated with the vorticity vector of the inlet boundary layer and formed what is called the passage vortex (PV). The other leg which formed behind (SLsl) is wrapping around the leading and then enters into the adjacent passage between the cascade blades. The sense of rotation of this leg is also determined by the vorticity of the inlet boundary layer and is opposite to the passage vortex in the passage between the cascade blades. The position of the saddle point of separation and its associated attachment and separation lines are important in defining the flow field near the end wall.

Figure 6 illustrates that the existence of the fence destroys the horseshoe vortex leg that formed behind the first separation line (SLpl) and forms two vortices with lower intensity than the original one formed without fence. In addition, as shown in figures 6 and 7 that in the case of using a fence, the fence works on breaking down the pressure leg of (HSV) which formed behind (SLpl), into two vortices having less intensive than pressure leg of (HSV). In the case of using fence there is no feed from the end wall flow to the corner vortex or passage vortex after middle of the passage. So, it appears that the passage vortex is weakened and no corner vortex is to be seen. Figure 7 shows the streamlines at the suction side wall of the blade in the case without using and with using fence. In case of using a fence, it is shown that the separation line which feeding from the boundary layers on the end wall is weaker, this resulted in a reduction of the channel vorticity strength and loss generation. The streamlines shown in figure 8 illustrate the flow uniformity improved by the addition of a fence in the channel cascade due to the reduction of the mixing losses.

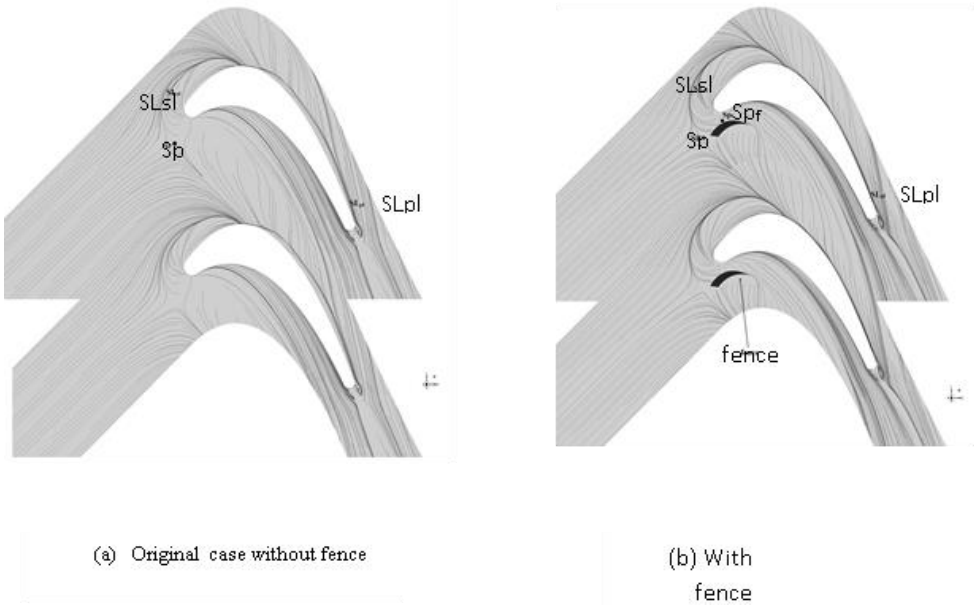

Fig. 6 Flow stream-lines visualization on the end wall without and with fence

4.3. Non-dimensional streamwise vorticity contours

Non-dimensional streamwise vorticity is shown in figure 9 for plane 3 (x = 0.144) behind the leading edge and for plane 12 (x = 1.4) in downstream. The effect of adding a fence is clearly shown when figure 9 (a) is compared to figure 9 (b). For plane 3 adding a fence in the passage create one of the vortices which is considered as the new pressure leg vortex of (HSV-pl), that interacts with the inlet boundary layer to form new passage vortex compared to the case without fence. The second vortex (FHSV-pl) generated after passing from fence rolled around new passage vortex in opposite direction of rotation (ccw as seen from exit

plane). More secondary vortices are generated with high intensity (compared with the case without fence) along spanwise direction as illustrated in figure 9 (a) and (b).

For plane 12 the case without fence the trailing edge shed vortices are created near the end wall side for both pressure (T-p) and suction (T-s) sides rotating in counter directions as in figure 9 (d), in the case with fence, the generated vortices in the pressure side (T-p) have intensity lower than the original case and the extension of the counter vortex (C-1) appears to be closer to the trailing edge shed vortex (T-p). The suction side vortex (T-s) has no significant intensity change and still in the counter rotation direction to the pressure side vortex. The vortex intensity in the end wall region is higher in the case without fence figure 9 (c) than the case with fence. The effect of adding a fence creates secondary vortex extension (T) in the downstream plane which rotates in counter direction to the extension passage vortex (P-1) resulted in a weak vortex if compared to the original case.

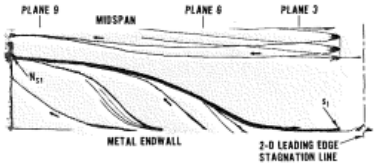

(a) Original case (measured) [4]

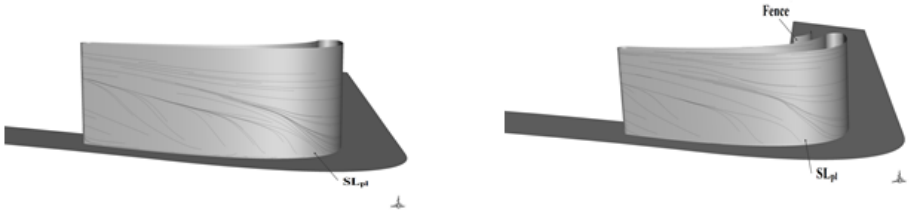

(b) Original case without fence (c) With fence

Fig. 7 Flow stream-lines visualization on blade suction side without and with fence

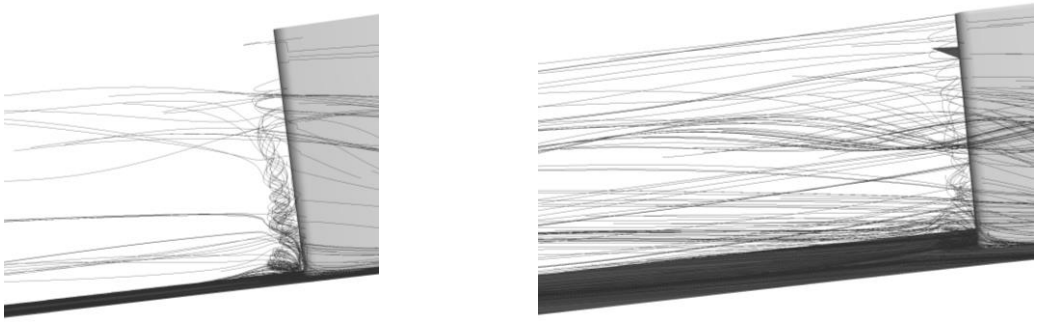

Without fence (a) (b) With fence

Fig. 8 Flow stream-lines visualization after trailing edge without and with fence

4.4. Static pressure coefficient (C_p) distribution

The pressure field inside the passage plays a major role on the shape of the horseshoe vortex and hence on the static pressure coefficient (C_p) contours close to the end wall, as shown in figure 10. The minimum pressure channel vortices on the end wall no longer occur at the blade suction side, as it exists for potential flow, but it moved into the channel between the two blades. Near the leading edge of the blade, the location of maximum pressure in the

channel corresponds to the location of the saddle point of separation, (Sp). The contours show a strong negative pressure gradient towards the suction surface in a parallel direction to the separation streamline. This is the region of creation of the separation vortex that locates at the saddle point of separation (Sp) and that eventually interacts with the blade suction Surface. In case of using a fence, a small change in the static pressure contour near the fence and separation point (Sp). Also, the existence of the fence makes a change in the pressure field that leads to the movement of (Sp) from its location in original case (at (x = -0.05, y= 0.82) to a new location at (x = -0.0552, y= 0.8). A new saddle point (Sp_f) located at (x=0.041, y=0.89) appears between the fence and the pressure side (PS) of the blade.

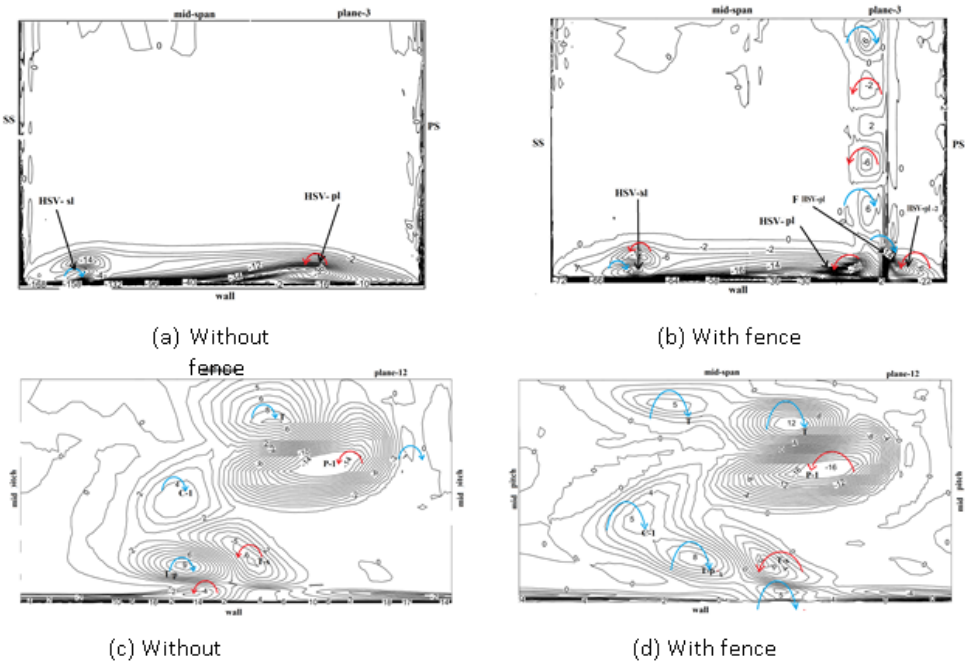

Fig. 9 non-dimensional streamwise vorticity at plane 3 and 12

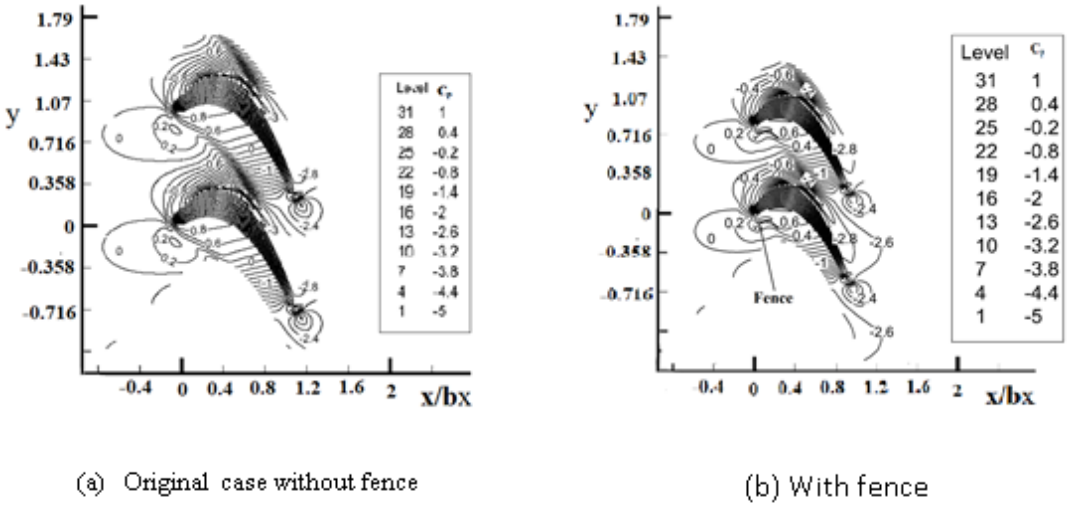

Fig. 10 Static pressure coefficient (C_p) distribution at end wall for the original case without fence and with fence

4.5. Flow Field results

Figure 11 illustrates the distribution of total pressure coefficient C_{pt} across planes 3, 6, and 9 in case of without using and with using fence which represents the locations of losses

initiated through the cascade. In plane 3, located just downstream from the saddle point of separation (Sp), the loss distribution remains characteristic of the collateral inlet boundary layer. The curled of the inlet boundary layer is evident adjacent to the channel pressure side, appearing as a high loss region. Another core of high loss, located close to the suction side, indicates the presence of a leg of the separation vortex originating from the saddle point (Sp) in the adjacent channel. As previously mentioned, the fence disrupts and weakens the (HSV) of pressure leg, which originates at (Sp). The fence is strategically located at the center of this (HSV) pressure leg, effectively altering its dynamics.

Figure 11(b) shows the measured and calculated loss distribution in plane 6. Here, the inlet boundary layer has rolled up, forming a vortex that interacts with the boundary layer on the suction side. In the case of the fence existence, a slight increase in the generated loss is observed at the center of the passage vortex (PV). This is attributed to the excessive friction generated by the fence; however, this is counterbalanced by a significant reduction in losses at the corner vortex compared to the original case. The fence affects the direction of the streamlines and the vortex formation. In plane 9, before the exit plane of the passage cascade, the loss distribution is presented in figure 11(c). At this location, the passage vortex (PV) increased substantially in size. High losses are prominent on the end wall adjacent the suction corner, where the end wall boundary layer separates at (SLpl), and on the suction surface where the (PV) interacts with the boundary layer of the blade. For the fence configuration in plane 9, the extent of the passage vortex within the channel is reduced compared to the original case. The vortex center shifts, resulting in lower losses when compared to the original case, and its height is also reduced. Additionally, the pitch-wise extent of the vortex is less pronounced, contributing to overall improved flow characteristics.

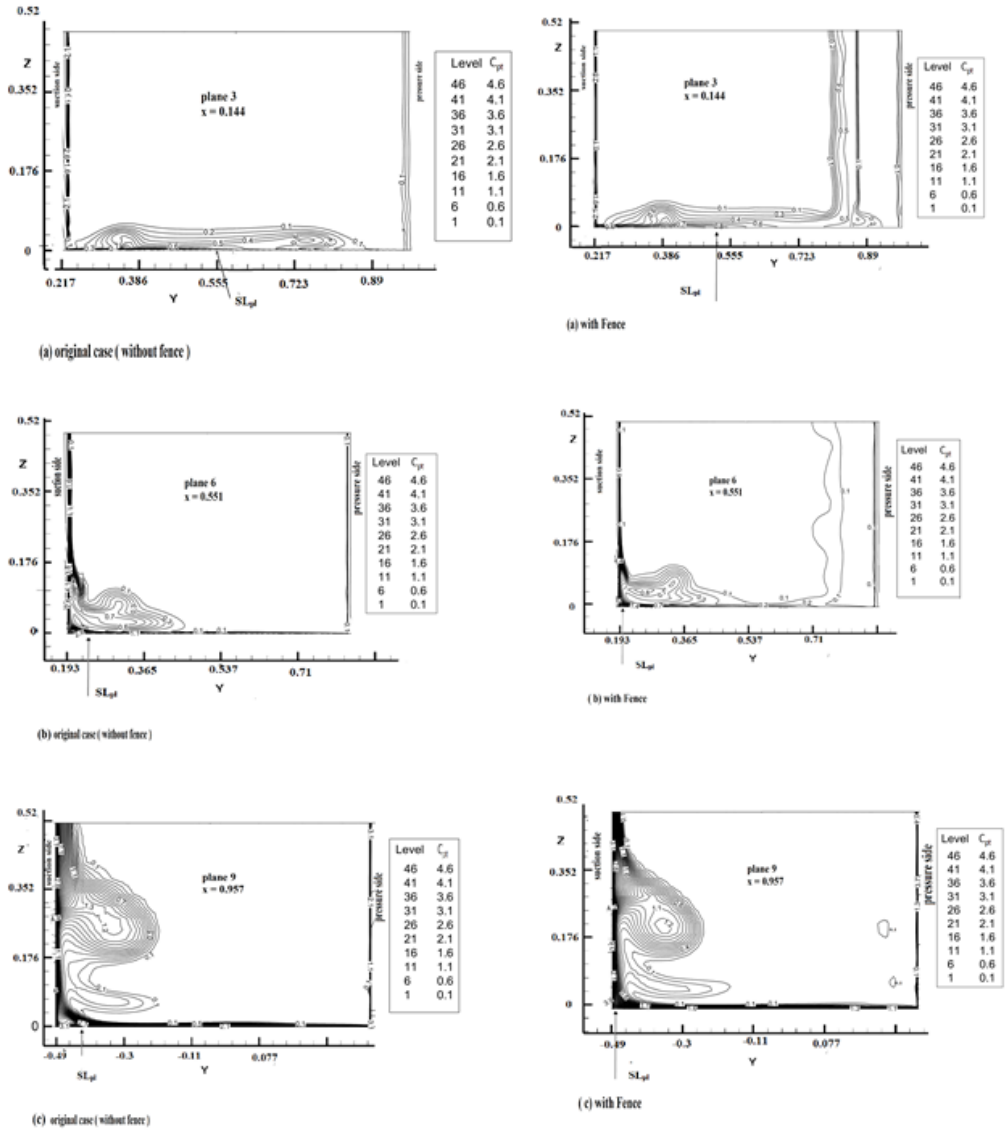

Fig. 11 Calculated total pressure loss coefficient at plane 3, 6, and 9 without fence and with fence

4.6 . Secondary Flow vectors

Three-dimensional flow in turbine blade cascades is characterized by primary and secondary flow components. The primary flow, is defined as the inviscid potential flow, follows idealized streamlines unaffected by viscous forces. In contrast, secondary flow arises due to viscous effects and boundary layer interactions, deviating from the primary flow. Figure 12 illustrates the velocity vector components in plane 7 and 8, in plane 7 revealing the secondary flow structure and its deviation from potential flow. The motion of the passage vortex is clearly visible, closely aligning with the center of the closed lines of the total pressure coefficient shown in figure 11.

In plane 8, depicted in figure 12, the flow field clearly shows the different regions of the passage vortex, counter vortex, and corner vortex. In the suction side region, at end wall corner, there is a small corner separation region bounded by the separation line (SLpl) and an attachment line on the suction surface. This region corresponds to the high corner losses observed in figure 11. When the fence is present, as shown in figure 12, the counter vortex is notably absent. This is due to the disruption of pressure leg of the (HSV) by the fence, which effectively eliminates the counter vortex and modifies the overall secondary flow structure.

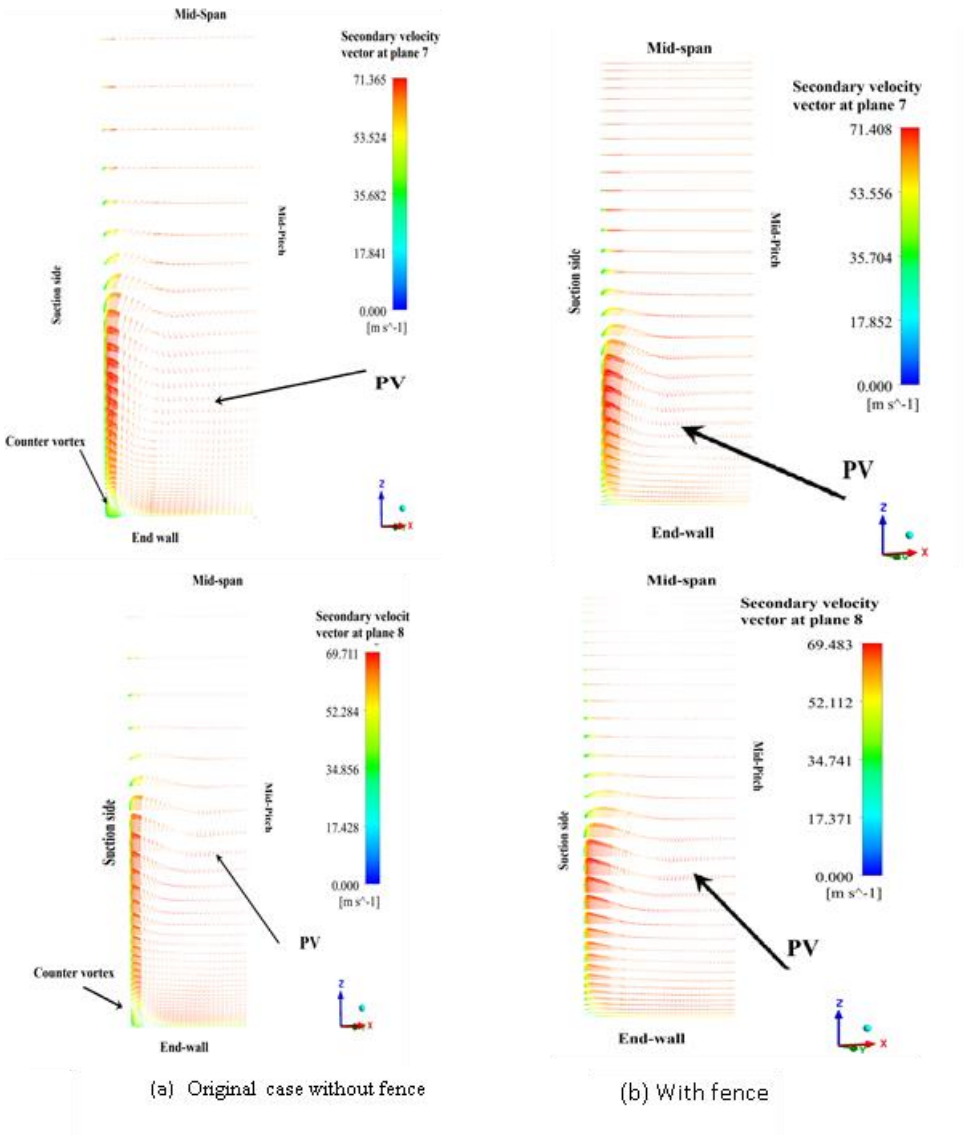

Fig. 12 Secondary flow at planes 7 and 8 without and with fence

The integrated loss coefficient through the cascade passage exhibits interesting trends. Figure 13 shows that the losses increased only slightly up to plane 6 compared to that found in plane 1. This minor increase is primarily caused by shear effects resulting from the three-dimensional roll-up of the inlet boundary layer and the development of the boundary layer downstream of the separation line (SLpl). Beyond plane 6, the losses increase more significantly due to two key phenomena. First, the separation vortex originating from (Sp) interacts with the suction surface boundary layer, creating suction surface separation. Second, the flow close to the suction surface crosses the throat and goes into a region of deceleration where the passage vortex increases in size. These factors combine to cause a rapid rise in the losses downstream of plane 6, as depicted in figure 13. Between planes 9 and 10, another significant rise in losses occurs due to flow separation at the blade trailing edge. Beyond the channel cascade, in planes 10, 11, and 12, the integrated mass averaged losses increase as the flow severe mixes downstream.

In the case of fence existence, a slight rise in the losses is observed from the leading edge to plane 6 compared to the original case. This increase may be attributed to the disruption of the (HSV), changes in the pressure field, or additional friction introduced by the fence. However, beyond plane 6, the fence significantly affects the losses reduction. This is

achieved through the breakdown of the (HSV) pressure leg, which reduces the intensity of the secondary flow. Additionally, the motion of the cross-passage flow from the pressure side to the suction side is minimized, and subtle changes in the static pressure field help control the pressure gradient. Furthermore, the fence weakens both the counter vortex and the corner vortex, resulting in a marked reduction in secondary flow losses.

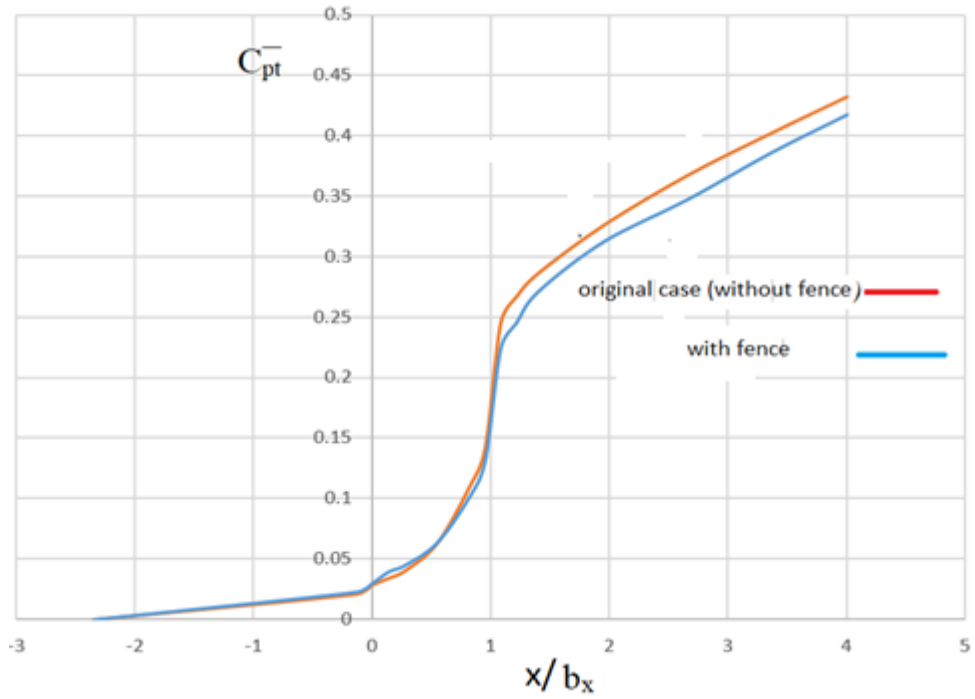

Fig. 13 Mass-averaged total loss coefficient as a function of axial distance through the cascade without fence and with fence

5. Conclusions

This study highlights the significant impact of cascade passage geometry modifications on the aerodynamic performance of Langston turbine cascade. Using validated CFD simulations in ANSYS Fluent 2023 R1, the introduction of a fence near the saddle point of the cascade passage has shown a reduction in the total pressure losses and improved the flow uniformity. Specifically, the fence decreased the total pressure loss coefficient by 5.244% at plane 12 compared to the original. The fence is intended to block the secondary flow development, thus reducing the development of the extensive low-energy flow zone at the blade's trailing edge. The most of the losses occur after exiting the cascade which is known as the mixing losses. In the present study, the flow uniformity is improved and hence the mixing losses are remarkably reduced. Moreover, the fence blocks the cross flow at the end wall and divide the end wall vorticity, leading to a reduction in the total secondary losses.

The fence effectively disrupted the horseshoe vortex and modified the pressure field, leading to a weakened passage vortex and suppressed the strength of secondary flows. Flow visualizations confirmed enhancement of the flow uniformity and reduced vortex strength, with improvements in the aerodynamic efficiency of the cascade. These results indicate the

potential of geometric modifications, such as fences, in reducing secondary flow losses and enhance turbomachinery performance.

Nomenclature

b_x	axial chord, mm
C_p	static pressure coefficient, $(P-P_o)/ (0.5\rho_o U_o^2)$
C_{pt}	total pressure coefficient, $(P_{to}-P_t)/(0.5\rho_o U_o^2)$
$\overline{C}_{pt}$	mass averaged total pressure coefficient
I	turbulence intensity, %
P	pressure, kPa
u	velocity, nondimensionalized on U_o
U_o	upstream inlet velocity to cascade, m/s
x	Coordinate normal to cascade leading edge, nondimensionalized on b_x
y	Coordinate parallel to cascade leading edge, nondimensionalized on b_x
y^+	non-dimensional wall distance
z	Coordinate perpendicular to end wall, nondimensionalized on b_x

Subscripts

o	upstream
t	total
x	component in *x*- direction

Abbreviations

ccw	counter clock wise
F	fence
HSV	horseshoe vortex
LE	leading edge
MS	midspan
pl	pressure leg
PS	pressure side
PV	passage vortex
RANS	Reynolds-Averaged Navier–Stokes
Sl	separation line
sl	suction leg
Sp	saddle point of separation
SS	suction side
STP	stander temperature and pressure
TE	trailing edge

Greek Symbols

β_1	airfoil mean camber line inlet angle, measured from Y axis
β_2	airfoil mean camber line exit angle, measured from Y axis
ρ	density

References

[1] Denton, J.D., Loss mechanisms in turbomachines. Vol. 78897. 1993: American Society of

Mechanical Engineers.

[2] Cho, J.-J., K.-S.J.J.o.t.K.S.f.A. Kim, and S. Sciences, Controlling the Horseshoe Vortex by the Leading-Edge Fence at a Generic Wing-Body Junction, Journal of Korean Society, 2009. 37(4): p. 336-343.

[3] Langston, L. S., Secondary flows in axial turbines—a review, Annals of the New York Academy of Science, 2001. 934(1): p. 11-26.

[4] Langston, L., M. Nice, and R. Hooper, Three-dimensional flow within a turbine cascade passage, J, Eng, Power, 1977. Vol. 99, pp. 21-28

[5] Langston, L., Crossflows in a turbine cascade passage, J. Engineer for Power, 1980. 102, pp. 866–874.

[6] Ryong, K.S. and J. Moon Young, Counter-Rotating Streamwise Vortex Formation in the Turbine Cascade with Endwall Fence, Computers and Fluids, 1999: p. 155-161.

[7] Govardhan, M., A. Rajender, and J.J.J.o.T.S. Umang, Effect of streamwise fences on secondary flows and losses in a two-dimensional turbine rotor cascade, J. Thermal Science, 209. 15: p. 296-305.

[8] Nandan Kumar, K. and M.J.J.o.F.E. Govardhan, On topology of flow in a turbine cascade, Jouranal of FLuids Engineering, 2014. 136(8): p. 081201.

[9] Adeola S. Shote, Gazi I. Mohamed, Josua P. Meyer, Influences of large fillets on endwall flows in a vane cascade with upstream slot film-cooling, Experimental Thermal and Fluid Scienc, 2020. 112: p. 109951.

[10] Cui, T., Wang, S, Tang, X., Wen, F., Wang, Z., Effect of leading-edge optimization on the loss characteristics in a low-pressure turbine linear cascade, J. of Thermal Science, 2019. 28: p. 886-904.

[11] Aunapu, N.V., Volino, R. J., Flack, K. A., and Stoddard, R. M.., Secondary flow measurements in a turbine passage with endwall flow modification, J. Turbomachines, 2000. 122(4): p. 651-658.

[12] Miao, X., Zhang, Q., Wang, L., J., Qi, H., Application of riblets on turbine blade endwall secondary flow control, Aerospace Research Central, 2015, V31(6): p. 1578-1585.

[13] Ingram, G., Gregory, D., Rose, M., Havey, N., Brennan, G., The effect of end-wall profiling on secondary flow and loss development in a turbine cascade in Turbo Expo: Power for Land, Sea, and Air, ASME, 2002.

[14] Ingram, G., Gregory, D., Rose, M., Havey, The benefits of turbine endwall profiling in a cascade, J. of Power and Energy, 2005. 219(1): p. 49-59.

[15] Nho, Y.C., P, J. S., Lee, Y. J., Kwak, J. S., Effects of turbine blade tip shape on total pressure loss and secondary flow of a linear turbine cascade, Int. J. of Heat and Fluid Flow, 2012. 33(1): p. 92-100.

[16] Li, X., Ji, L., Zhou, L., Numerical research on the trailing-edge sweep of supersonic/transonic turbines, Aerospace Science and Technology, 2020. 99: p. 105696.

[17] Halder, P. and P.M.J.O.e. Kumar, Coupled CAD-CFD automated optimization for leading and trailing edge of an axial impulse turbine blade, Ocean Engineering, 2020. 213: p. 107769.

[18] Ansys Fluent Theory Guide, ANSYS, Inc. Release 2021 R2 Southpointe July 2021 2600 Ansys Drive Canonsburg, PA 15317 ANSYS, Inc. and ansysinfo@ansys.com Ansys Europe, Ltd. are UL http://www.ansys.com

[19] Ahmed Abdelnaby Abdelhameed; Saleh Abo-Elfadl Ahmed; Othman Hassan Othman; Abdel Moneim Mahmoud Ibrahim. "Influence of using Straight and Twisted Elliptical Section Heater Tubes on Stirling Engine Performance". JES. Journal of Engineering Sciences, 50, 6, 2022, 11-30. doi: 10.21608/jesaun.2022.150787.1155

[20] Ahmed Ibrahim; Othman Hassan; Mohamed El-Dosoky; Moahmed Abdelghany. "Numerical Investigation of Film Cooling Effectiveness and Flow Field Characteristics over a Flat Plate with in-Hole Swirl Generator". *JES. Journal of Engineering Sciences*, 51, 6, 2023, 53-80. doi: 10.21608/jesaun.2023.221981.1244

[21] Ahmed Hussien; Ahmed Ali; Ibrahim Ismail. "Comparative Investigation of the Energy Efficiency of Mini-Split Air Conditioning with Variable Refrigerant Flow Systems for Office Buildings in Hot Climate.". *JES. Journal of Engineering Sciences*, 52, 2, 2024, 52-72. doi: 10.21608/jesaun.2024.244895.1276